Impact Resistant Polymeric Glasses Using Compressive Pre-Stress

Jared S. Archer, Alan J. Lesser

Department of Polymer Science and Engineering, University of Massachusetts, Amherst, Massachusetts 01003

Received 12 January 2009; accepted 15 March 2009
DOI 10.1002/app.30440
Published online 17 August 2009 in Wiley InterScience (www.interscience.wiley.com).

ABSTRACT: The application of an externally applied pre-stress on impact properties is studied on polymethyl methacrylate (PMMA) organic glass. Samples are tested under equi-biaxial compression, simple shear and a combination of biaxial compression and shear. Equi-biaxial compression is shown to increase the threshold stress level for projectile penetration whereas shear pre-stress has a large effect on the overall energy absorbed during an impact. There is also an apparent interaction observed between compression and shear to dramatically increase the threshold stress. Pre-stressed laminates show an increase in damage area because of the unique formation of a secondary cone. Higher levels of compressive equi-biaxial pre-stress significantly increase the stress relaxation time because of the corresponding increase in hydrostatic stress.
 J Appl Polym Sci 114: 3704–3715, 2009

Key words: re-stress; PMMA; composites; fracture; impact resistance

INTRODUCTION

The development of transparent materials that are more impact and ballistic resistant have many possible applications ranging from military vehicle windows to civilian products such as hurricane resistant windows. Two common organic glasses that are used in these applications include polycarbonate (PC) and polymethyl methacrylate (PMMA). These materials are transparent and are more lightweight when compared with their inorganic counterparts, which is important especially in vehicle and personal protection applications. Each of these materials has a unique mechanism by which energy is absorbed during impact. PC, like other ductile materials, has the ability to absorb large amounts of energy through yielding. In the case of PMMA, the majority of energy absorption is because of the creation of surface area during fracture. There is a stark difference between the macroscopic failure mechanisms of these two materials. Failure in PC is relatively localized while PMMA is effective at delocalizing failure in the form of radial cracking and Hertzian cone fracture (during impact).

The effect of loading rate is also an area where these two materials differ. At low velocity impact rates, PC outperforms PMMA while at ballistic rates the V_{50} (velocity at which the probability of failure is 0.5) of PMMA can exceed that of PC.[1,2]

The continual goal in materials science is the improvement of the performance of materials to meet applications. In the case of brittle materials, one way to improve their working range is through the application of compressive pre-stress. The idea of using a compressive pre-stress to enhance the properties of non-polymeric brittle materials has been used with success for quite some time.[3] The use of concrete in structures is made more feasible by the application of a compressive pre-stress through either pre or post-tensioned tendons. In concrete, the tensile strength is very low when compared with its compressive strength consequently a superposed compressive stress can greatly increase the working stress range of the material. Inorganic glasses have also been shown to display improved strength when tempered because of an induced layer of compression on each surface of the glass.[4] The ballistic response of ceramic targets pre-stressed by confinement on all surfaces by titanium or steel was modeled by Holmquist and Johnson.[5] In the case of complete penetration, pre-stress was shown to decrease the exit velocity of the projectile. When only partial penetration was obtained, the extent of penetration was decreased by pre-stress. Similar experimental work by Bao et al. looked into the effects of pre-stress and confinement on ceramic targets.[6] Multi-axial compressive pre-stress was applied to heated alumina tiles by the shrinkage of an aluminum alloy cast around the tile. Critical failure loads

Correspondence to: A. J. Lesser (ajl@polysci.umass.edu).

were determined by contact of a steel ball on a free surface of alumina under biaxial pre-stress. A 15-fold increase was observed for both the critical load at quasi-static rates as well as the critical impact energy at low velocity rates.

Work has also been done to investigate the effect of pre-stress on polymeric materials. Motahhari and Cameron used an approach similar to pre-stressed concrete by applying a pre-tension to glass fibers during cure to place an epoxy matrix under uniaxial compression.[7] They found a 33% increase in impact energy absorbed during Charpy tests. The improvement was explained by residual shear stresses weakening the fiber matrix interface promoting failure in the longitudinal direction. However, the increase in impact properties showed an apparent upper limit because of the weakening of the fibers by residual tensile stresses. Fancey also studied fiber reinforced polymeric composites. Here, the pre-stress was applied to a thermosetting polyester matrix by imbedding pre-tensioned nylon 6,6 fibers before cure. In contrast to the work by Motahhari and Cameron, Fancey used the visco-elastic recovery of fibers to apply the pre-stress.[8] The rational behind this approach was to address some of the challenges with the fabrication of non-planar geometries. Fancey observed a similar improvement of 25% in impact energy with charpy tests.

One approach to the fabrication of armors relies on the synergistic relationship between brittle and ductile layers. A clear example of the effectiveness of this approach is in composites of PC and PMMA. Hsieh and Song studied composites of alternating layers of PC and PMMA where the thickness of each component was on the micron length scale.[9] It was determined that the critical parameter in the ballistic response of these composites was the thickness of the PMMA. The brittle layer thickness determined the amount of damaged area. When failure is delocalized by PMMA it allows a larger volume of the backing PC layer to participate in yielding and hence increase the performance. Hsieh and Song illustrated this effect nicely by comparing laminates with mm scale thickness of equivalent corresponding ply thicknesses of PC/PC/PC to PC/PMMA/PC. The laminate that incorporated the brittle interlayer showed a 37% increase in V_{50}.[2]

In this work, we will look at some interesting changes in failure mechanism that occur when the PMMA layer of these laminates is subjected to a compressive pre-stress. In contrast to the aforementioned methods of pre-stress, this work uses methods of pre-stress that maintain transparency of the target. To the authors' knowledge, all the work on polymers has focused on uniaxial pre-stress with beam geometries. This work focuses on the effects of biaxial pre-stress. Both equi-biaxial and more complicated stress states are investigated. The damage initiation, mechanisms, and sequence are reported for both conventional and pre-stressed laminates as well as for monolithic plates. Also the stress relaxation of equi-biaxially pre-stressed plates is compared with uniaxial stress relaxation.

EXPERIMENTAL PROCEDURE

Materials

The principal material under investigation was Acrylite PMMA obtained from McMaster-Carr. The material was supplied in two forms: rectangular sheets and circular samples with a nominal diameter of 102 mm. The nominal thickness of both forms was 6 mm. The as-received PMMA showed no noticeable birefringence suggesting that residual stresses due to processing are negligible. The elastic properties of the PMMA were measured according to ASTM D638. Young's modulus, E, was 3.29 GPa and Poisson's ratio, ν, was 0.33. PC sheets with a thickness of 3 mm from McMaster-Carr were also used in the fabrication of laminates. Methylene Chloride was obtained from Sigma-Aldrich and used without purification. Polyurethane adhesive was likewise purchased from McMaster-Carr.

Application of pre-stress

Two methods of pre-stress application were used. One was a square frame made of one-inch steel bar stock (Fig. 1). In the frame bolts at each corner are tightened to apply compressive stress in the glass. Depending on the initial sample geometry, this frame allows for application of shear, biaxial compression, or a combination of the two. In the case of biaxial compression, samples were machined as $63.5\times$ 63.5 mm^2 squares. In an attempt to obtain a state of equi-biaxial compression at the center, the sample was viewed between crossed polars during loading. If extinction is achieved at a point in a specimen under load regardless of rotation, then every direction in the plane at that point is a principal direction and the stress is equi-biaxial.[10] The level of pre-stress was measured by a foil strain rosette mounted on the surface of the sample in the center.

In the case of simple shear, samples were machined to a rhombus and deformed in the frame to a square. The angle machined into the samples was used to estimate the level of shear pre-stress (Fig. 2).

The other method of pre-stress used a shrink fit technique. A carbon steel pipe was cut into a 12 mm thick ring and the inner diameter was bored out so that it was smaller than the 102 mm diameter of a disk of PMMA at room temperature [Fig. 3(a)]. The

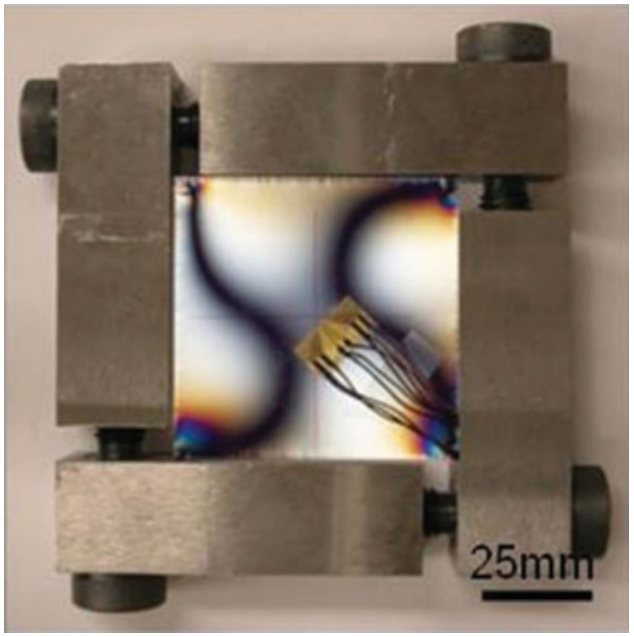

Figure 1 Square frame with overlaid image of pre-stressed sample viewed under crossed polars. Scale bar = 25 mm. [Color figure can be viewed in the online issue, which is available at www.interscience.wiley.com.]

radial mismatch between the inner radius of the steel ring and the PMMA disk ranged from 0.26 to 0.42 mm. The PMMA was cooled down in liquid nitrogen shrinking the disk to a diameter smaller than the steel ring. The shrunken disk was fit inside of the steel ring and upon warming to room temperature a seal pressure developed on the sample. This type of loading condition produces an equi-biaxial stress state throughout the specimen. The image of a shrink fit sample viewed between crossed polars in Figure 3(b) shows extinction throughout the sample regardless of rotation because every direction is a principal direction. The level of pre-stress can be

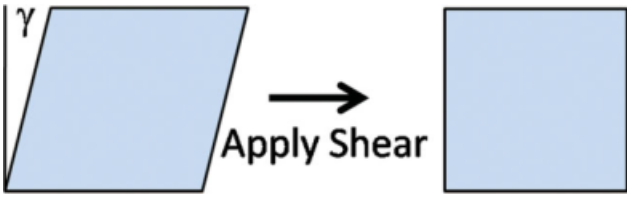

Figure 2 Schematic of simple shear pre-stress method. [Color figure can be viewed in the online issue, which is available at www.interscience.wiley.com.]

determined by considering the radial displacements of the two components according to eq. (1), which is derived from Lamé's classical solution.[11]

$$\sigma_{rr} = \sigma_{\theta\theta} = \delta\left[\frac{a}{E_m}\left(\frac{a^2+b^2}{b^2-a^2}+\upsilon_m\right)+\frac{a}{E_p}\left(1-\upsilon_p\right)\right]^{-1} \quad (1)$$

The radial mismatch, δ , is the difference between the radius of the PMMA disk and the inner radius of the metal ring at room temperature before assembly. The parameters a and b are the radii of the PMMA after assembly and the outer radius of the ring after assembly, respectively (Fig. 4). E and υ are the modulus and Poisson's ratio and the subscripts p and m refer to the polymer and metal ring, respectively. The modulus of the steel was measured to be 200 GPa by a ring compression test, whereas the value of 0.29 for Poisson's ratio was estimated from the average value of 1955 grades of carbon steel.[12,13] In all cases, pre-stress was applied at 23° C before testing.

Transparent composite laminates with a PC/PMMA/PC architecture were fabricated by either solvent welding with methylene chloride or by a commercial polyurethane adhesive. Each surface of each ply was cleaned with isopropyl alcohol. In the case of solvent welding, the PC ply was partially submerged in a shallow dish of methylene chloride for 10 s then pressed onto the PMMA ply. Pressure

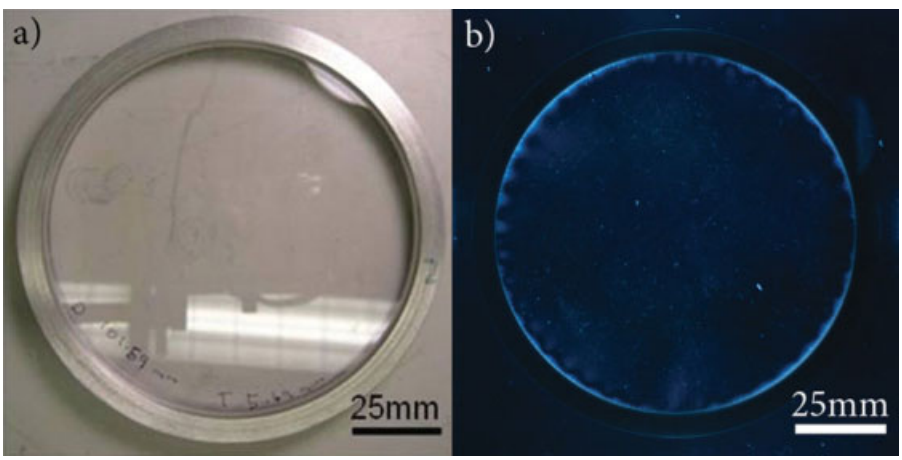

Figure 3 (a) Shrink fit sample. (b) Shrink fit sample viewed between crossed polars. Scale bars = 25 mm. [Color figure can be viewed in the online issue, which is available at www.interscience.wiley.com.]

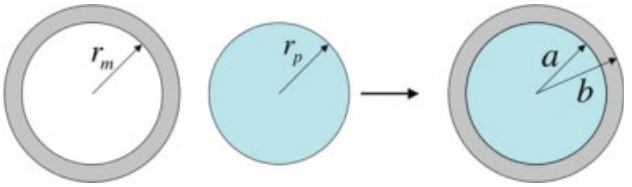

Figure 4 Dimensions used in shrink fit calculations. [Color figure can be viewed in the online issue, which is available at www.interscience.wiley.com.]

was then applied by a toggle clamp for 3 min and the solvent was allowed to evaporate overnight. The polyurethane used was a two part adhesive that was mixed with a static mixer. The adhesive was applied to one ply and the other ply was pressed by hand to yield an interlayer thickness on the order of 0.25 mm. The method of pre-stress used on the laminates was exclusively shrink fit. The incorporation of PC plies necessitates higher velocities to achieve failure in the laminates. The impact velocity was chosen so that it was high enough to create damage in the laminate but low enough that the tup base did not impact the sample. At these velocities, the tup does not fully penetrate the sample i.e. all the kinetic energy is absorbed in each test.

Low-velocity impact testing was conducted on a Dynatup 8250 with a 6 mm diameter tup and a hammer mass of 3.256 kg. The capacity of the load cell was 44 kN. Impact velocities ranged from 3 to 6 m/s. The 3–4 m/s range was achieved in gravity mode whereas the 4–6 m/s range required pneumatic assist. The sample was secured during testing via a pneumatic clamp with a force of 1.64 kN. To insure consistent boundary conditions for different methods of pre-stress, steel shaft collars with an inner diameter of 42 mm were placed on each surface of the sample to directly transfer the load of the clamp to the sample. High-speed images were captured during impact tests by a Kodak Ektapro HS Motion Analyzer model 4540 with frame rates up to 40,500 fps.

Impact tests at ballistic rates were performed at the Army Research Laboratories in Natick, MA. The apparatus used was a helium gas gun firing a 17-grain projectile. The experiments referred to here were performed at ~130 m/s (near the V_{50} of 6 mm PMMA).

Average roughness, R_a, was measured using a Veeco Dektak 150 profilometer with a 12.5 μm radius stylus. The value R_a is defined for a line scan of length L in the x direction as the average deviation in the y direction from the mean line defined by $y = 0$.

$$R_a = \frac{1}{L}\int_0^L \left|y\right| dx \tag{2}$$

For each area under investigation, three 500 μm scans were made under a 98 μN force at a rate of 16.6 μm/s. Measurements were made on the radial crack surface of shear pre-stressed samples in the center of the thickness and as near the point of impact as possible.

The viscoelastic response of PMMA was probed with stress relaxation experiments. Type I ASTM tensile bars were machined from 6 mm sheets using a Tensilkut fixture and router table. Uniaxial tensile stress relaxation was performed on an Instron 5800. The change in load with time was measured on a 50 kN capacity load cell using Instron's Merlin software. Temperature was controlled by a Thermcraft oven and temperature controller. The series of temperatures used to construct a master curve were: 25, 30, 40, 50, 60, 70, 80, 90, and 100° C. The reference temperature for shifting the data was 25°C. For biaxial stress relaxation, the shrink fit method was used. The change in stress with time was measured by applying a strain gage on the outer surface of the steel ring in the θ direction. The stress in the PMMA can then be calculated using Hooke's law and the elasticity equations for a cylinder with internal pressure.[11]

$$\sigma_r = \sigma_\theta = \frac{\varepsilon_\theta}{2}\left[\frac{\nu_m E_m}{(1+\nu_m)(1-2\nu_m)} + \frac{E_m}{(1+\nu_m)}\right]\left[\left(\frac{b}{a}\right)^2 - 1\right] \tag{3}$$

Here, a and b refer to the inner and outer radii of the steel ring, respectively. The temperature was controlled by placing the assembly inside a polyethylene bag then placing the bag inside a water bath maintained at 25 ± 1° C.

RESULTS AND DISCUSSION

Low-velocity failure mechanism

Although investigating the response of monolithic plates under low-velocity impact rates, one of the first observations made on the effect of pre-stress was an apparent change in failure mechanism (Fig. 5). Samples without pre-stress display radial cracking that extends beyond the boundary of the clamps as well as cone fracture. When a compressive pre-stress is applied, the only clearly visible mechanism is cone fracture. High-speed photography was used during impact to observe the development of each mechanism. From the images, it was determined that radial cracks were indeed formed in pre-stressed samples but the growth of the cracks was stunted so that the radius of the cone exceeded the length of the radial cracks (Fig. 6). In a general sense, this initial observation appears to be negating one of the most beneficial aspects of failure in PMMA. Namely, the amount of delocalization of damage area apparently decreases with the

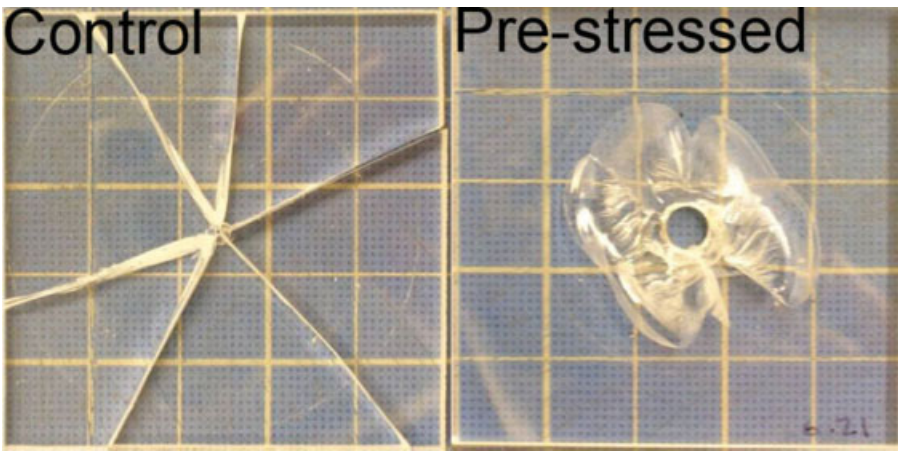

Figure 5 Low velocity (~ 2 m/s) failure mechanism. In the control sample, the dominant mechanism is radial cracks. Under pre-stress, cone fracture is most visible. Underlying grid unit = 12.7 mm. [Color figure can be viewed in the online issue, which is available at www.interscience.wiley.com.]

application of pre-stress. However, this apparent disadvantageous failure mechanism will take a different advantageous form as will be discussed in the section on transparent laminate composites.

High-velocity failure mechanism

Some preliminary results from ballistic tests on pre-stressed monolithic plates of PMMA suggest there are at least some similarities between the effects of pre-stress at low and high velocities. The failure mechanism of the control sample is largely dominated by radial cracking with a small vestige of Hertzian cone fracture (Fig. 7). The opposite is observed in the pre-stressed sample. Damage is localized with a prominent Hertzian cone while radial cracking is suppressed. Further work is needed to establish whether or not other trends (such as an increase in threshold) observed at low velocities are also seen at ballistic rates.

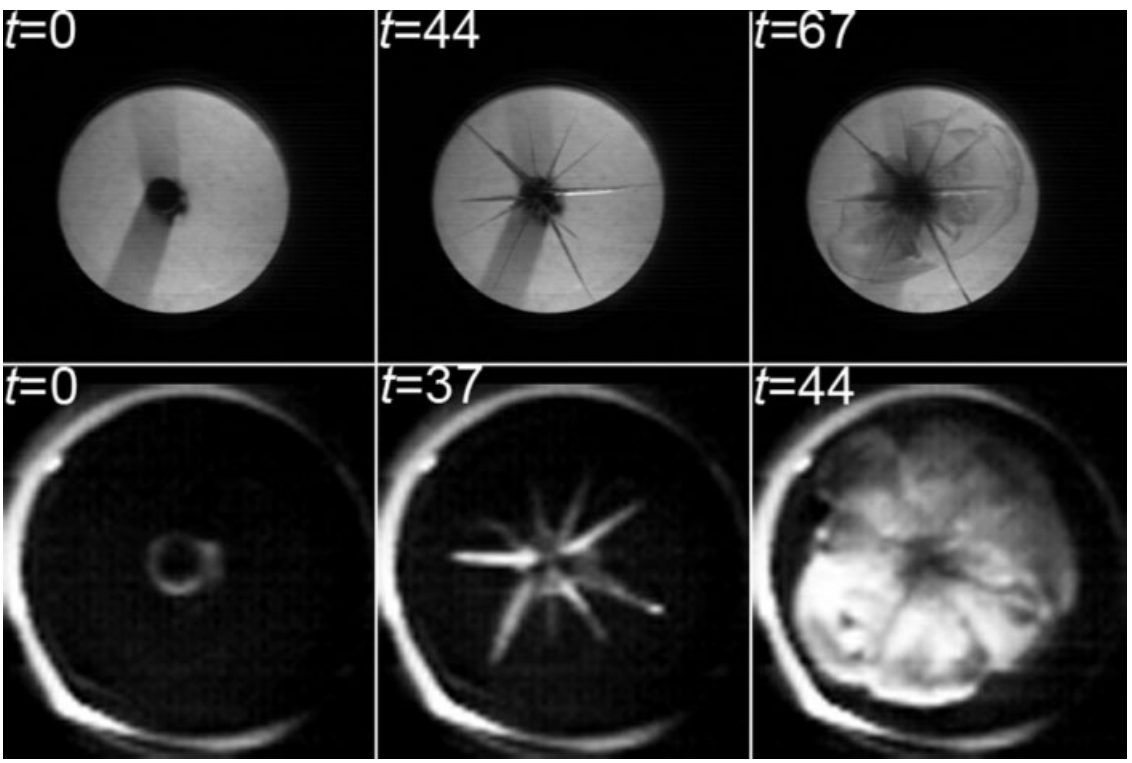

Figure 6 Low velocity mechanism change. Top row (frame rate = 4500 fps) - control sample exhibits large radial cracks as well as cone fracture. Bottom row (frame rate = 40,500 fps) - pre-stressed sample shows stunted radial crack growth. Unit of time = ms. Diameter of circular boundary in all images = 42 mm.

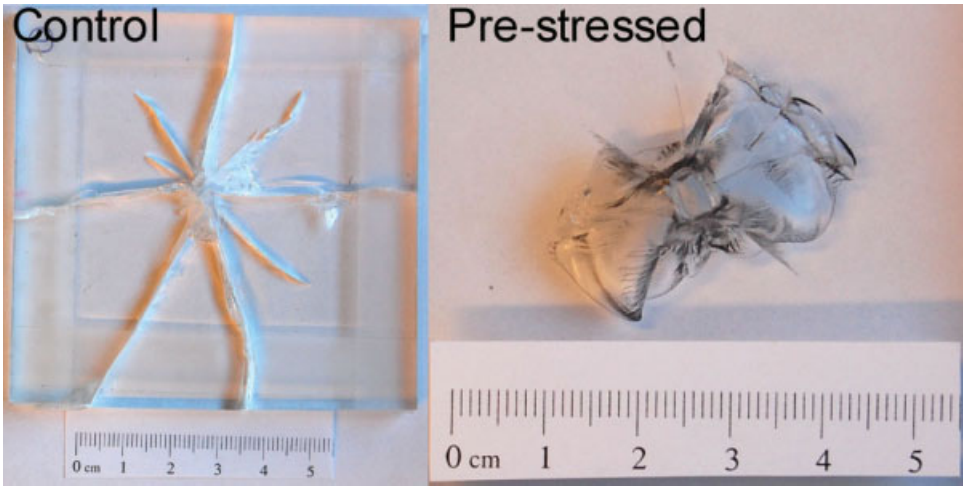

Figure 7 Ballistic impact (~ 130 m/s) on monolithic plates. Significant reduction of radial cracking seen with pre-stress. [Color figure can be viewed in the online issue, which is available at www.interscience.wiley.com.]

Impact energy

When looking at the total impact energy of pre-stressed PMMA, the improvements are modest. The average value of impact energy for the shrink fit method increases from 0.71 J/mm to 0.92 J/mm whereas the square frame method shows increases from 0.96 J/mm to 1.25 J/mm, an ~ 30% increase in impact energy for both pre-stress methods (Fig. 8). This increase in impact energy is somewhat surprising given the initial observation that pre-stress seems to localize damage resulting in less created surface area. This observation coupled with the fact that brittle materials absorb energy by surface area creation would lead one to expect a decrease in impact energy with a decrease in created surface area. To investigate this apparent discrepancy, the high-speed images were compared with the load deflection curves to get estimates on the amount of energy required to create the separate features.

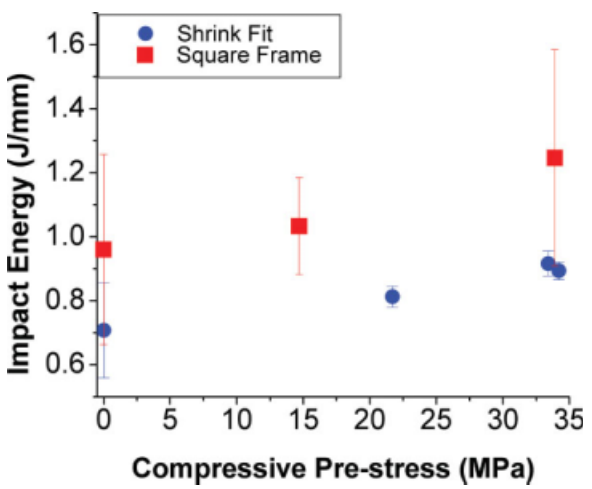

Figure 8 Effect of pre-stress on impact energy. [Color figure can be viewed in the online issue, which is available at www.interscience.wiley.com.]

Estimates of the surface area created during cone fracture were made by analyzing images of fractured samples. For the radial crack surface area on control samples, a penetrant dye was used to mark the initial surface area then the sample was fractured in liquid nitrogen to separate each piece (Fig. 9). For pre-stressed samples, although cone fracture removes most of the evidence of radial cracks, the ends of the cracks are still visible and can be located by analyzing the high-speed images. Since direct measurements were not possible, the shape was assumed to be triangular, which is likely an overestimate of the surface area. By assuming that radial cracking initiates at the point of nonlinearity in the load - deflection curve, the high-speed images were synchronized with the load – deflection data to determine at which point the different mechanisms began and ended. The energy was calculated by integrating the load - deflection curve over the limits defined in eqs. (4), (5), and Figure 10 and subtracting off the area under the theoretical unloading curve. The unloading curve travels linearly to the origin based on the assumption that plastic deformation

Figure 9 Radial crack surface area for energy estimates. Sample thickness = 5.75 mm. [Color figure can be viewed in the online issue, which is available at www.interscience.wiley.com.]

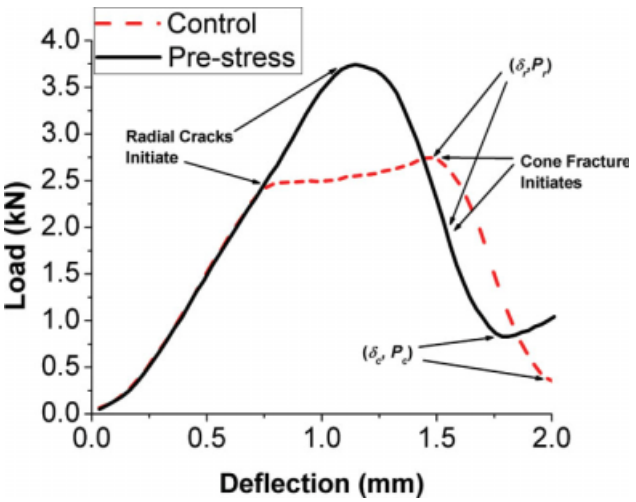

Figure 10 Comparative load - deflection curve. Failure mechanism initiation observed by high speed photography.[Color figure can be viewed in the online issue, which is available at www.interscience.wiley.com.]

during fracture is negligible for brittle materials such as PMMA.

$$E_r = \int_0^{\delta_r} P(\delta) d\delta - \frac{1}{2}\,\delta_r\,P_r \tag{4}$$

$$E_c = \int_0^{\delta_c} P(\delta) d\delta - \frac{1}{2}\,\delta_c\,P_c - E_r \tag{5}$$

where, E_r = Energy absorbed by radial fracture mechanism; $P(\delta)$ = Load as a function of displacement; δ_r = Final deflection for radial fracture mechanism; P_r = Final load for radial fracture mechanism; E_c = Energy absorbed by cone fracture mechanism; δ_c = Final deflection for cone fracture mechanism; P_c = Final load for cone fracture mechanism.

In the control samples, fracture energies were estimated to be 0.6 ± 0.1 kJ/m^2 and 1.1 ± 0.3 kJ/m^2 to create radial cracks and cone surfaces, respectively. With a pre-stress of ~33 MPa, the energy to create radial cracks increased dramatically to 2.8 ± 0.6 kJ/m^2 whereas the energy for cone fracture remained relatively unchanged at 0.9 ± 0.1 kJ/m^2. This significant increase in the energy for radial cracks can be explained by considering two observations. One, which has already been mentioned, is that pre-stress stunts radial crack growth resulting in less surface area. The other is that the peak or threshold load reached in pre-stressed specimens is significantly higher than the control, which leads to an increase in energy (Fig. 10). The combination of more energy and less surface area explains this drastic increase. The modest increases in total impact energy are a consequence of normalizing the energy by sample thickness rather than created surface area.

It is interesting to note the relative scatter in the impact energy data (Fig. 8). The lowest amount of scatter occurs in shrink fit samples. Both the control samples and the square frame pre-stressed samples have greater variation in absorbed energy. It appears that an added benefit of a uniform state of pre-stress is greater reproducibility, which is beneficial from an applications design standpoint.

The comparison of the load - deflection curves in Figure 10 illustrates an important consequence of an externally applied pre-stress. In the control sample, following initiation of radial cracking, the load gradually increases with increasing deflection until cone fracture initiates and the load drops. In the pre-stressed sample, the load drops dramatically upon radial crack initiation. The pre-stressing process stores strain energy in the PMMA. As the plate begins to deflect during impact, the strain energy can be released by impact promoted buckling, which is evidenced by the drop in load. It is important to note that this trend is attributed to the specific method of pre-stress application. If the pre-stress were applied by a laminated architecture, the laminate would be self-stabilizing. Any buckling of a compressively pre-stressed ply would come at the penalty of adding strain energy to the tensile pre-stressed ply.

Threshold

One of the beneficial effects of pre-stress shown in Figure 10 is the increase in the failure threshold. This effect was quantified in two ways. In the first method, the threshold was determined by sequentially increasing the drop height until complete penetration occurred. Without pre-stress, a drop-height of 195 mm (4.9 J) resulted in penetration. With the application of 31 MPa in the square frame the threshold was increased to 396 mm (9.9 J). The second method involved a single specimen approach. The threshold load was defined as the highest load before irreversible damage as indicated by the departure from linearity in the load-deflection curves. This load was, in turn, used to define the threshold stress

$$\sigma_t = \frac{P}{h^2}(1+\upsilon)\left[0.485\ln\frac{a}{h} + 0.52\right] \tag{6}$$

where, P is the threshold load, h is the thickness, ν is Poisson's ratio and a is the clamped radius.[14] The threshold stress is the maximum tensile stress, from bending, on the surface opposite impact. As is seen in Figure 11, the threshold stress increases with pre-stress. In the case of the shrink fit samples, the increase in threshold stress is approximately equal to the pre-stress on the sample. This is an expected result, if the increase in threshold is from simple

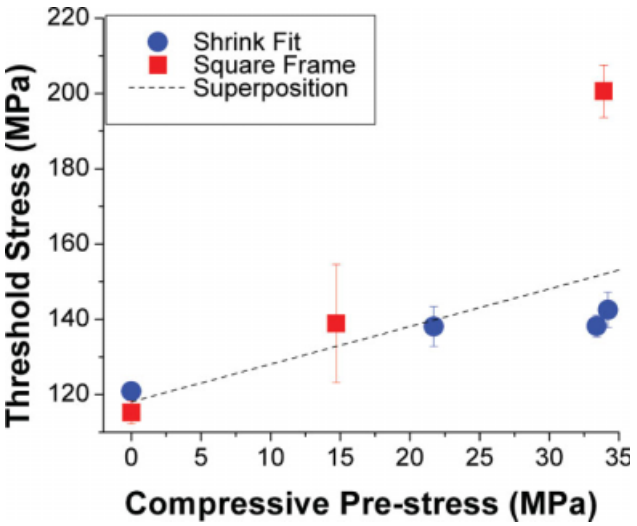

Figure 11 Effect of pre-stress on threshold. [Color figure can be viewed in the online issue, which is available at www.interscience.wiley.com.]

superposition of the pre-stress. However, samples pre-stressed in the square frame deviate significantly from this trend in that they show a dramatic increase in the threshold stress. This observed difference is significant and is an area of continuing research. The main difference of the two methods of pre-stress lies in the state of stress in the sample. In the case of shrink fitting, the sample is in equi-biaxial compression throughout the plane. The square frame induces some level of shear stress in addition to the biaxial compression as evidenced by the presence of isochromatic fringes seen between crossed polars (Fig. 1).

Effect of shear

Samples under simple shear pre-stress exhibit a fracture pattern indicative of the state of stress in the sample. The dominate feature is one large radial crack aligned normal to the principal tensile stress direction. The cone fracture has an elliptical projection with its major axis parallel to the radial crack. Fractography of the radial crack surface reveals circular features near the point of impact that turn into parabolic markings at points further from the center (Fig. 12). These patterns give witness to the formation of secondary cracks ahead of the primary crack front and are indicative of a high level of stress at the crack tip.[15,16] These surface features have a rough appearance, which was quantified by profilometry (Fig. 13). Not only are there finer surface features being created, but the initiation of these secondary cracks will occur at local heterogeneities and is not necessarily confined to a single plane. As the primary crack front proceeds, it will change direction to meet the secondary cracks. This change in direction along with the increase in surface area suggests an increase in energy absorbed during failure, which is indeed observed in Figure 14. For a sample under simple shear pre-stress, the first principal stress adds to the tensile stress due to bending of the plate during impact resulting in a decrease in the threshold stress. It is clear from these results that simple shear alone cannot account for the increase in threshold seen for samples pre-stressed in the square frame.

Pre-stressed transparent composite laminates

As mentioned above, the laminates were tested at velocities that resulted in arrest of the tup regardless of sample composition and pre-stress level. However, interesting effects of pre-stress can be seen by observing the resultant fracture patterns. The two different methods of adhering the plies give interfaces with different strengths, and the strength of this interface plays an important role in the performance of the laminate. When solvent welding is used the interface is relatively strong compared to the strength of the interface formed with the polyurethane adhesive. A most interesting result is observed in pre-stressed solvent welded laminates. In addition to radial cracking and cone fracture, a large secondary cone is formed in the PMMA ply (Fig. 15).

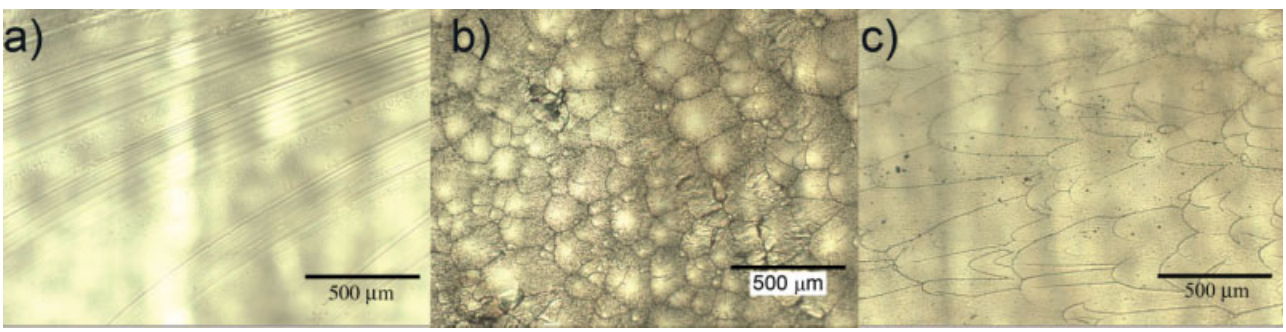

Figure 12 Fractography of radial crack surface for (a) shrink fit sample, (b) shear pre-stressed sample near impact, and (c) shear pre-stressed sample away from impact. All scale bars = 500 μm. [Color figure can be viewed in the online issue, which is available at www.interscience.wiley.com.]

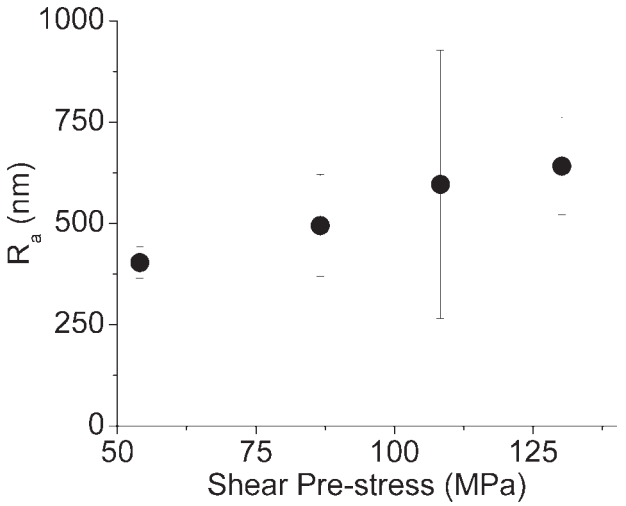

Figure 13 Surface roughness of radial cracks on shear pre-stressed samples.

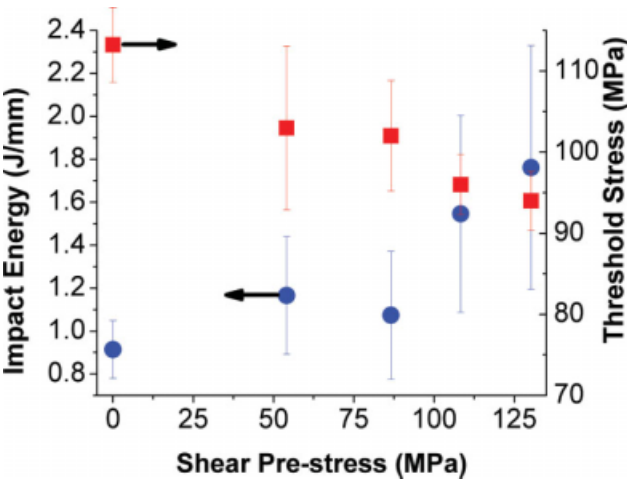

Figure 14 Effect of shear pre-stress on impact energy and threshold. [Color figure can be viewed in the online issue, which is available at www.interscience.wiley.com.]

The secondary cone initiates at the impacted surface and grows radially toward the distal surface of the ply at a shallow angle. All of the damage created by the secondary cone is confined to the PMMA ply. As seen in Figure 15, the radius of the secondary cone slightly exceeds the 21 mm radius of the clamp. Work done by Hseih and Song has shown that when impact velocities are increased to ballistic rates and thicker samples are tested, the V_{50} of PMMA exceeds that of PC.[2] If damage in the PMMA ply absorbs more energy than the PC ply then the formation of a large secondary cone would drastically improve performance at ballistic rates. This secondary cone is not observed in control samples (Fig. 16).

A negative effect of a strong interface can also be seen in Figure 15. Sharp radial cracks are initiated in the PMMA ply, and because of the high strength of the interface, the cracks are able to propagate through the back ply of PC. This is disadvantageous for two reasons. The cracks form in the PC without significant yielding, which should decrease the amount of energy absorbed. Also, the cracked portions peel open allowing PMMA spall to pass. This latter issue would be especially important in transparent armor applications where containment of spall is necessary to protect personnel. When the polyurethane adhesive is used between plies, the failure process changes significantly from that observed in the solvent welded laminates. The

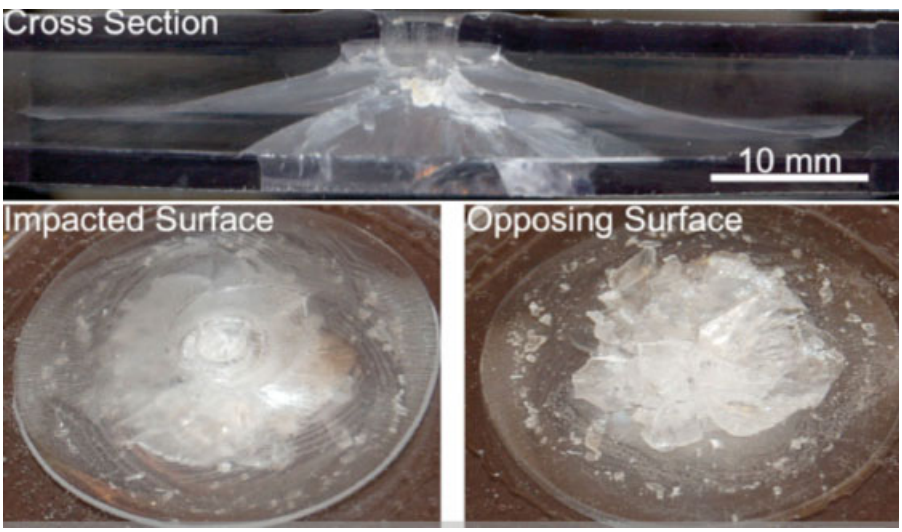

Figure 15 Top image cross section of PC/PMMA/PC laminate using solvent welding on both plies showing secondary cone and brittle fracture of PC distal ply. Bottom images PC/PMMA/PC laminate using solvent welding on impacted ply and polyurethane on opposing ply shows secondary cone as well as containment of PMMA spall (cone diameter $\sim$ 50 mm). [Color figure can be viewed in the online issue, which is available at www.interscience.wiley.com.]

Figure 16 Control laminate - no secondary cone formation. [Color figure can be viewed in the online issue, which is available at www.interscience.wiley.com.]

secondary cone seen in pre-stressed solvent welded laminates does not occur when the top ply is adhered to the PMMA by polyurethane. With the weaker interface at the back ply, sharp cracks from the PMMA ply do not propagate into the PC. The failed interface maintains the continuity of the PC ply containing spall.

Relaxation

When considering applications where the amount of pre-stress determines the end use properties, it is important to know how the pre-stress will change with time. To address this concern, the viscoelastic response of PMMA was characterized under uniaxial and equi-biaxial stress relaxation (Figs. 17 and 18). The nominal initial stress for the uniaxial tests was 24 MPa, whereas the nominal stress levels for the equi-biaxial tests were 28 and 17 MPa. A master curve was assembled from the uniaxial relaxation data according to the procedure for the method of reduced variables as outlined by Ferry.[17] The WLF parameters were calculated by plotting log a_T vs. $(T\text{-}T_0)/(T\text{-}T_\infty)$, where T_∞ was chosen such that a linear fit through the data passed through the origin.[17,18] The slope of the linear fit is equal to c_1 =28.01 and $c_2 = T_0\text{-}T_\infty = 147.6$ K, where $T_0 = 298.15$ K and

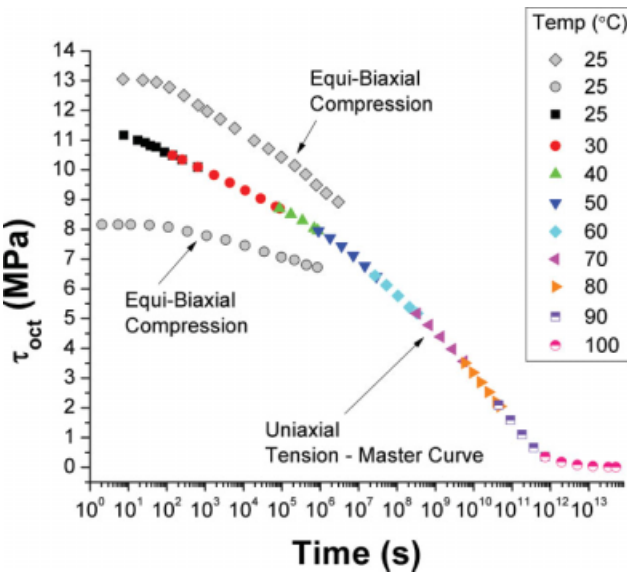

Figure 18 Octahedral shear stress relaxation for both uniaxial tension and biaxial compression. Uniaxial tension is represented by a master curve. [Color figure can be viewed in the online issue, which is available at www.interscience.wiley.com.]

T_∞ = 150.6 K (Fig. 19). These values are found in Table I. Attempts were made to construct a master curve of stress relaxation in shrink fit samples, however difficulties were encountered. When the temperature was raised, the added thermal expansion of the PMMA caused the disks to buckle so that the relaxation response could not be measured accurately. The room temperature equi-biaxial relaxation data, although not as extensive as the master curve, is plotted alongside the uniaxial tensile stress relaxation data for comparison (Fig. 18). The stress relaxation response was characterized by fitting the

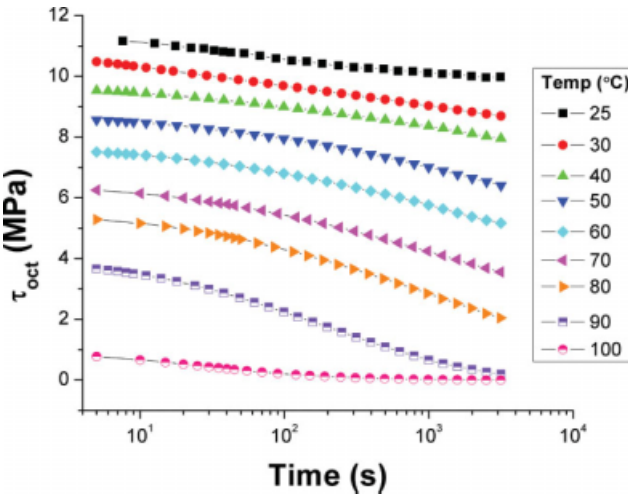

Figure 17 Octahedral shear stress relaxation for uniaxial tension. [Color figure can be viewed in the online issue, which is available at www.interscience.wiley.com.]

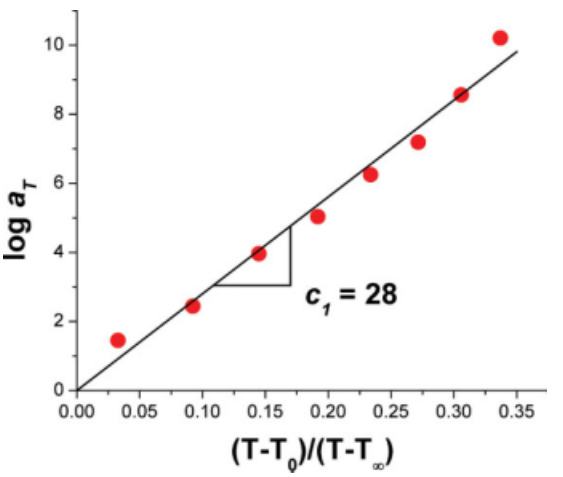

Figure 19 Calculation of WLF parameter c_1. [Color figure can be viewed in the online issue, which is available at www.interscience.wiley.com.]

TABLE I
WLF Parameters and Relaxation Times for Uniaxial and Equi-biaxial Stress Relaxation

	τ_{oct} (MPa), $t = 0$	σ_m (MPa), $t = 0$	c_1	c_2 (K)	T_∞(K)	τ_1(s)	τ_2(s)
Uniaxial	11.4	8.0	28	148	151	455 ± 99	89,600 ± 16,600
Equi-biaxial	8.2	−11.5	–	–	–	1,330 ± 400	111,000 ± 27,800
Equi-biaxial	13.2	−18.7	–	–	–	1,800 ± 399	388,000 ± 90,300

data to a two-parameter exponential decay of the form:

$$\tau_{oct}(t) = y_0 + A_1 e^{\frac{-t}{\tau_1}} + A_2 e^{\frac{-t}{\tau_2}} \quad (7)$$

For the uniaxial data, only the initial portion of the master curve ($t = 0$, $t = 10^6$ s) was analyzed to compare to the available equi-biaxial data (Table I).

Both equi-biaxial samples have relaxation times that are from 1.2 to 4.3 times higher than the uniaxial relaxation times even though one is at a higher stress level and the other is at a lower stress level with respect to the uniaxial case. The interesting result shown in Table I is that the relaxation times increase for higher levels of equi-biaxial pre-stress. A comparison can be made between the uniaxial and equi-biaxial relaxation times by linearly interpolating between the two equi-biaxial data sets to $\tau_{oct} = 11.4$ MPa. When this is done the relaxation times for the equi-biaxial case are a factor of three greater than the uniaxial case.

We can gain further understanding of these results by comparing the hydrostatic stress (σ_m) and the octahedral shear stress (τ_{oct}) for uniaxial tension and equi-biaxial compression. For uniaxial tension, let $\sigma_{11} = \sigma_0$ and for equi-biaxial compression, let $\sigma_{11} = \sigma_{22} = \sigma_{0.}$ For these conditions, $\sigma_m = \sigma_0/3$ for uniaxial and $\sigma_m = -2\sigma_0/3$ for equi-biaxial. It should be noted that, for a given value of σ_0, the octahedral shear stress is identical for uniaxial and equi-biaxial loading, $\tau_{oct} = \sqrt{2}\sigma_0/3$. Also, the corresponding values for the hydrostatic stress are opposite in sign and differ by the value of σ_0. Another significant difference between these two stress states is that the magnitude of the hydrostatic stress for the equi-biaxial case is twice that of the uniaxial case and increases more rapidly than the octahedral shear stress for increases in σ_0. Typically, as τ_{oct} and σ_m are increased, relaxation times are decreased.[19,20] The shear stress drives the change in shape while the hydrostatic stress accelerates the process for $+\sigma_m$ and decelerates the process for $-\sigma_m$. For uniaxially loaded members, increases in σ_0 increase bothτ_{oct} and σ_m so one would expect relaxation times to decrease with higher levels of σ_0. In contrast, increases in σ_0 for the equi-biaxial state of stress increase τ_{oct} and decrease σ_m. These observations give insight into the curious result for the equi-biaxial state of stress where increased relaxation times are observed for a higher level of τ_{oct} (Table I). The increasing hydrostatic compression retards the stress relaxation at higher levels of σ_0 since its magnitude has a greater effect on the relaxation time than the corresponding increase in shear stress. This is an important result, especially for transparent armor applications, since higher levels of biaxial prestress will not only have better impact performance but will also relax more slowly.

Additionally, this experimental approach provides a clean way to probe the effect of hydrostatic stress on relaxation. An example of this is the work by Lu and Knauss who studied the effect of dilation on creep using annular samples of PMMA subjected to mutiaxial loading in the form of torsional and uniaxial loading.[20] One issue with the interpretation of their data arises when comparing the response of a specimen under only shear loading to one that has the same shear load in addition to an axial load. If the applied shear stress is the same, the superposed axial load adds an additional amount to τ_{oct} so that the observed result is a composite response to changes in τ_{oct} and σ_m. If uniaxial and equi-biaxial tests are run at the same value of σ_0, τ_{oct} will be the same and any differences in the response will be due to the changes in σ_m.

CONCLUSIONS

Pre-stressing PMMA affects several aspects of the impact response of the material. A decrease in damage area is seen at both low velocity and ballistic rates for monolithic plates. Radial crack growth is suppressed leading to higher apparent fracture energies. Total impact energy is increased by $\sim$ 30% for both methods of pre-stress. The threshold stress is increased by an amount consistent with superposition for equi-biaxially pre-stressed samples. When the glass is subjected to a complicated state of prestress involving both shear and biaxial compression, the increase in threshold stress is substantially greater. The application of simple shear pre-stress leads to the formation of secondary cracks ahead of the primary crack front and a subsequent increase in the total impact energy. With the laminates tested, pre-stress interestingly led to the formation of a secondary cone in the brittle PMMA layer with a radius that exceeded the clamped boundary. The stress

relaxation experiments highlighted the important role of hydrostatic stress in the stress relaxation process. When the mean stress was compressive, increases in relaxation times followed. This important result suggests that specimens subjected to higher levels of compressive pre-stress will not only perform better under impact but will also retain these improvements for longer times.

The authors are grateful for the help of John Song.

References

1. Lewis, G.; Mladsi, S. Biomaterials 2000, 21, 775.
2. Hsieh, A. J.; DeSchepper, D.; Moy P.; Dehmer, P. G.; Song, J. W. ARL-TR-3155 (2004).
3. Freyssinet, E. U.S. Patent #2,080,074, 1937.
4. Minor, J. E. APT Bull 2001, 32, 47.
5. Holmquist, T. J.; Johnson, G. R. J Phys IV Fr 2003, 110, 597.
6. Bao, Y.; Su, S.; Yang, J.; Fan, Q. Mater Lett 2002, 57, 518.
7. Motahhari, S.; Cameron, J. J Reinf Plast Compos 1998, 17, 123.
8. Fancey, K. S. J Reinf Plast Compos 2000, 19, 1251.
9. Hsieh, A. J.; Song, J. W. J Reinf Plast Compos 2001, 20, 239.
10. Dally, J. W.; Riley, W. F. Experimental Stress Analysis; McGraw-Hill: New York, 1991.
11. Saada, A. S.Elasticity Theory and Applications; Krieger: New York, 1993.
12. Frisch-Fay, R. Flexible Bars; Butterworths: Washington DC, 1962.
13. http://www.matweb.com.
14. Timoshenko, S.; Woinowsky-Krieger, S.Theory of Plates and Shells; McGraw-Hill: New York, 1959.
15. Beardmore, P.; Fellers, J. Mater Sci Eng 1969/70, 5, 120.
16. Bhattacharjee, D.; Knott, J. F. Int J Fracture 1995, 72, 359.
17. Ferry, J. D.Viscoelastic Properties of Polymers; John Wiley & Sons: New York, 1980.
18. Williams, M. L.; Landel, R. F.; Ferry, J. D. J Am Chem Soc 1955, 77, 3701.
19. Gol'dman, A. Ya.; Demenchuk, N. P.; Murzakhanov, G. Kh. Mech Compos Mater 1989, 24, 707.
20. Lu, H.; Knauss, W. G. Mech Time-Dep Mater 1999, 2, 307.